AIAA-2003-4062
Transonic Aerodynamics of a Wing/Pylon/Strut Juncture

Andy Ko, W.H. Mason and B. Grossman
Virginia Polytechnic Institute and State University
Blacksburg, VA

21st AIAA
Applied Aerodynamics Conference
23-26 June 2003 / Orlando, FL

Transonic Aerodynamics of a Wing/Pylon/Strut Juncture

Andy Ko*, William H. Mason† and Bernard Grossman‡

Multidisciplinary Analysis and Design (MAD) Center for Advanced Vehicles
Virginia Polytechnic Institute and State University
Blacksburg, VA 24061-0203

The Multidisciplinary Analysis and Design (MAD) Center at Virginia Tech investigated the strut-braced wing (SBW) design concept for several years. Our studies found that SBW configurations had savings in takeoff gross weight of up to 19% and in fuel weight of up to 25% compared to a similarly designed cantilever wing transport aircraft. In our work we assumed that computational fluid dynamics (CFD) could be used to achieve target aerodynamic performance levels. However, no detailed CFD design was done. This paper uses CFD to study the transonic aerodynamics of the wing/pylon/strut juncture of an SBW configuration. This is the critical aspect of the aerodynamic design. The goal was the reduction or elimination of interference drag at this juncture. Inviscid CFD analysis has been used to investigate the flow characteristics at this juncture. Initial results showed the presence of strong shocks at the juncture. Our analysis showed that the strut/wing intersection was behaving like a two-dimensional nozzle between the bottom of the wing and the top of the strut, choking the flow at the minimum area point and expanding the flow downstream resulting in a strong shock near the trailing edge of the strut. We also found that the pylon did not have a major influence on the flow characteristics at the wing/pylon/strut intersection. Geometry changes were made to reduce the shock strength at the wing/pylon/strut intersection, eliminating the nozzle effect. Results showed that this design effectively reduced the shock strength and in some cases eliminated it.

1. Introduction

The strut-braced wing (SBW) design concept has been studied by the Multidisciplinary Analysis and Design (MAD) Center at Virginia Tech for several years. The configuration considered was a 7500 nmi range transonic passenger transport aircraft. For this configuration the strut runs between the bottom of the fuselage to around the 67% semi-span location of the wing. The strut is connected to the wing via a pylon to increase the distance between the wing and the strut at the intersection. To avoid buckling, the strut adopts an innovative telescoping sleeve mechanism so that it only carries tension loads. From an aerodynamics standpoint, minimizing the interference drag between the wing, pylon and strut juncture is a key requirement in the aerodynamic design of the strut-braced wing airplane.

*Graduate student, Department of Aerospace and Ocean Engineering, Student Member AIAA. Email: yako@vt.edu.

†Professor, Department of Aerospace and Ocean Engineering Associate Fellow AIAA. Email: whmason@vt.edu.

‡Professor, Department of Aerospace and Ocean Engineering, currently Vice President, Education, National Institute of Aerospace, 144 Research Drive, Hampton, VA 23666, Fellow AIAA. Email: grossman@nianet.org.

1.1. Strut-Braced wing aircraft concept

The strut-braced wing design concept has been implemented in many general aviation aircraft. Although proposed by Pfenninger in the 1950s [1], the SBW concept has never been used on a transonic passenger transport aircraft. Early Virginia Tech MAD Center investigations by Grasmeyer et al. [2],[3],[4] found that the SBW configuration resulted in a wing with a higher aspect ratio and decreased wing thickness without any increase in wing weight relative to its cantilevered wing counterpart. The SBW configuration also has a lower wing sweep, allowing the wing to achieve some natural laminar flow without incurring a penalty in wave drag. Initial studies found that the SBW configuration had a 15% savings in takeoff gross weight (TOGW), 29% savings in fuel weight and a 28% increase in *L/D* compared to its cantilevered wing counterpart. Later, Lockheed Martin Aeronautical Systems (LMAS) did an evaluation of the work by the MAD Center. Refinements were made to the MDO code during this time, and it was found that a fuselage mounted engine SBW configuration showed a 9% savings in TOGW over a similarly designed cantilever wing aircraft design [5]. Further refinements were made, improving the optimization architecture [6], and wing structural weight prediction method [7]. The final

optimization results indicated that a wing-mounted engine SBW configuration had savings in TOGW of up to 19% and fuel weight savings of almost 25% over a similarly designed cantilever wing aircraft design [6]. Figure 1 shows the general layout of the different configurations considered in our studies.

a) Cantilever baseline design configuration

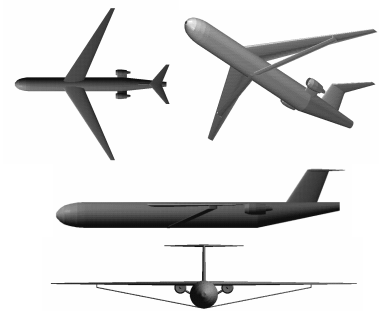

b) Fuselage mounted engine strut-braced wing design

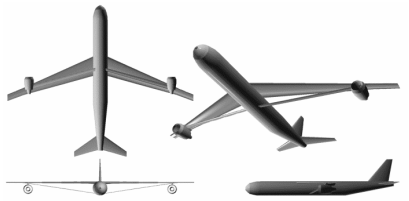

c) Wing mounted engine strut-braced wing design

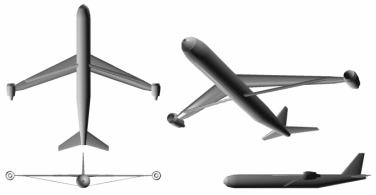

d) Tip mounted engine strut-braced wing design

Figure 1: General configuration layouts investigated in the Virginia Tech Strut-Braced Wing Design study [6].

In 1999, a flight demonstration of the SBW concept was proposed using a re-winged A-7 aircraft. This demonstrator aircraft would be used to prove the aerodynamic and structural feasibility of the SBW concept, including the innovative strut design that would take loads only in tension. Preparation for a flight vehicle demonstration required that a detailed aerodynamic investigation be made of the wing/pylon/strut intersection. Although our group had conducted fundamental CFD studies on wing/wall interference in anticipation of doing a detailed aerodynamic design [8], our MDO studies simply assumed that the juncture region could be designed for low interference drag using CFD. However, no actual aerodynamic design had been done.

1.2. Transonic interference drag for a wing/strut configuration

Although there have been few studies of the transonic interference drag of a wing/pylon/strut juncture arrangement, there has been research on wing-pylon and wing-body aerodynamic interference. Bartelheimer et al. [9] performed an experimental investigation of a strut placed normal to the wall of a wind tunnel, making pressure measurements along the span of the strut. Because the strut was near the tunnel walls, the data obtained was only suitable for Computational Fluid Dynamics (CFD) validation.

Potsdam et al. [10] performed an analysis and geometry refinement of a wing-pylon junction using two Euler flow solvers on unstructured grids. One of the flow solvers was coupled with an inverse design method. They presented guidelines on how to improve the wing-pylon flowfield. Their results were later validated with a flight test and Navier-Stokes computations.

For a wing-fuselage arrangement, Agrawal et al. [11] used Euler flow solvers to investigate the transonic flow at the wing/fuselage juncture to compare the accuracy of the solvers. They found that an implicit finite-volume upwind scheme provided the best results when compared to experimental data.

A comprehensive description of previous interference drag research was given by Tetrault in reference [12]. Tetrault then went on to carry out a fundamental CFD study of wing/wall transonic aerodynamic flowfield interference. This work was done to establish the foundations for our SBW studies. As part of his research, Tetrault found that an arched-shaped strut allowed the strut to intersect the wing perpendicularly, increasing the distance between the strut and the wing at the intersection. There was a drag reduction with an increasing arch radius. He also found that viscous forces tended to reduce the strength of the

shock induced near the wing/strut junction compared to predictions based on Euler calculations.

This paper describes a further investigation into understanding the flow physics at the wing/pylon/strut juncture at transonic speeds. In this investigation we examined the detailed aerodynamic design of the wing/pylon/strut intersection for the proposed flight demonstrator. We will present the results of design modifications made to the intersection design that shows how to reduce the shock strength at the juncture, thus reducing the interference drag.

2. Configuration Description

The A-7 SBW demonstrator aircraft consisted of a re-winged A-7 aircraft. The wing was chosen from our SBW design studies. It has a 29.3° leading edge sweep and an 11.4 aspect ratio. This is a lower sweep and a higher aspect ratio than a similarly designed cantilever wing aircraft. The wing was scaled for the A-7, maintaining the aspect ratio, taper ratio, thickness to chord ratios, wing sweep and wing loading. The placement of the scaled SBW wing was chosen to keep the static stability of the aircraft the same as that of the original A-7 aircraft. In doing so, the strut sweep had to be reduced from 19.4º to 4.1º to keep the strut from intersecting with the landing gear bay. We determined that this change in design did not impact the original qualities of the SBW design drastically [13]. Table 1 provides a summary of the dimensions of the wing used for the A-7 SBW demonstrator aircraft.

Table 1: Summary of the dimensions of the wing for the A7 SBW demonstrator aircraft

	A7 demonstrator wing
Wing Root chord	7.72 ft
Wing Tip chord	2.03 ft
Wing Root *t/c*	0.133
Wing Break *t/c*	0.062
Wing Tip *t/c*	0.075
Wing L_{LE}	29.28º
Wing Break *h*	0.67
Wing Area	270.8 ft^2
Wing Span	55.57 ft
Wing Taper Ratio	0.262
Wing Aspect Ratio	11.4
Strut Chord	1.58
Strut *t/c*	0.08
Strut L_{LE}	4.1º
Strut Span	37.25ft

Since no wing twist information was provided from the SBW studies, a baseline twist distribution was determined by using a vortex lattice design program [14] to find the spanload for minimum induced drag. Four wing stations were selected at which the wing twist was specified for the design. A straight-line wrap between these stations determined the twist distribution of the entire wing. The twist angles at these wing stations were tailored such that the twist distribution of the entire wing closely resembled the twist distribution prescribed by the linear theory solution.

In addition to the twist distribution, supercritical airfoils were also designed for the four wing stations. With the design two-dimensional lift coefficients, Mach number, and thickness to chord ratios obtained from the design load distribution and wing geometry definition, airfoil sections design for minimum drag were developed. These airfoils were based on the NASA supercritical airfoil family presented by Harris [15]. They were modified to meet the *t/c* requirements with low drag at the design point and maintain good off-design performance using MSES. This was done by manually reshaping the surface geometry. Details of the airfoil design work can be found in Reference [13].

The strut is attached to the bottom of the fuselage and connects to the wing via a pylon. The pylon is located at the 67% semi-span location of the wing and extends 4.1% semi-span below the wing. The strut has a *t/c* of 8%. An NACA 0008 airfoil was initially used for both the strut and the pylon, but was later changed to a SC(2)-0010 airfoil, scaled down to a *t/c* of 8% for each.

3. Design Approach

3.1. Computational Methods

Three analysis and design packages were used for this work. The first one, Rapid Aircraft Modeler (RAM) was used as a geometry CAD modeler to quickly produce and modify the required geometry for analysis. The FELISA system was the three dimensional analysis tool used as the CFD grid generator and flow solver. Both programs were provided to us by NASA Langley to perform the work. MSES was used for the airfoil analysis and design. Additional software to translate data between the two programs was written in-house.

3.1.1. Rapid Aircraft Modeler – RAM

The Rapid Aircraft Modeler, or RAM, was developed for the Systems Analysis Branch at NASA Ames. As the name suggests, it is a CAD tool that can be used to create three-dimensional objects of complete aircraft or aircraft systems. Since it is designed to create aircraft geometries, objects such as wings, tails, the fuselage and cockpit can be easily created. It also provides for the creation of flaps and slats, including control surfaces. Wing twist and dihedral can also be incorporated easily. Although RAM has only a small library of airfoils, it has a provision for use of custom

designed airfoils via an input file. RAM runs on any UNIX workstation with OpenGL support.

3.1.2. FELISA

The FELISA system was written by J. Peiro from the Department of Aeronautics at Imperial College, London, K. Morgan at the Department of Civil Engineering at the University College of Swansea at Swansea, U.K. and J. Peraire from the Department of Aeronautics and Astronautics at MIT for NASA Langley. It consists of an unstructured tetrahedral grid generator and an Euler equation flow solver using a Galerkin finite element method[16]. It also includes visualization tools to view the unstructured grid and flow solution, together with other post-processing software written by other FELISA users. For this application, all the data obtained from FELISA was post-processed and visualized using *Tecplot v8.0*.

3.1.3. MSES

MSES is a two dimensional airfoil analysis code. It solves the inviscid flowfield by modeling the steady Euler equations in integral form. An integral viscous formulation is used to model the boundary layers and wakes. The inviscid and viscous flowfields are solved simultaneously through a Newton-Raphson method. Further detail about MSES can be found in References [17] to [19].

3.2. Design Methodology

First we performed a CFD analysis of the baseline A-7 demonstrator aircraft geometry to observe and identify the key flow characteristics of the design. This led us to concentrate on the wing/pylon/strut intersection because the results showed the presence of strong shocks (hence contributing to large interference drag) at this intersection. To understand the flow physics at the wing/pylon/strut intersection, we decided that further analysis and design work would only model the wing, pylon and strut geometry, neglecting the fuselage. Comparative studies [13] indicated that due to the high aspect ratio wing, and the large distance of the intersection from the fuselage, the fuselage had a negligible effect on the flow at the intersection. Also, by concentrating only on the wing/pylon/strut configuration, we reduced our computational and setup time to an acceptable rate of one flow solution per day, as opposed to 1 to 1.5 weeks for the geometry with a fuselage.

To understand the flow occurring at the wing/pylon/strut juncture, we performed geometric parametric studies changing properties such as pylon toe and strut twist. The results from these studies provided us with the necessary insight to gain an understanding of the flow physics at the juncture. This led us to make design changes that reduced and in one case, eliminate the shock at this juncture.

4. Results

4.1. Initial Configuration

The first step was to model the entire A-7 SBW demonstrator aircraft and perform a CFD analysis to identify key design areas requiring concentration. Since this analysis was done early in the project, the supercritical airfoil design work done in parallel had not yet been completed. Therefore, baseline NASA supercritical airfoils obtained from Harris [16] were used in the wing and NACA 0008 airfoils were used for the strut and pylon. Hence, the results obtained from this analysis were interpreted with the consideration that better wing supercritical airfoils would be used later.

Figure 2 shows the geometry that was created in RAM that was to be used to in the analysis of the A-7 SBW demonstrator aircraft design. The surface triangulation of this grid is show in Figure 3. Using this grid, a FELISA inviscid flow solution was obtained at a Mach number of 0.85.

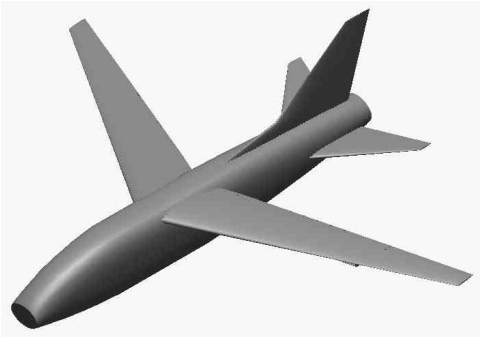

Figure 2: Rendered picture of the simplified A-7 SBW demonstrator aircraft geometry modeled in RAM used to generate in the computational grid.

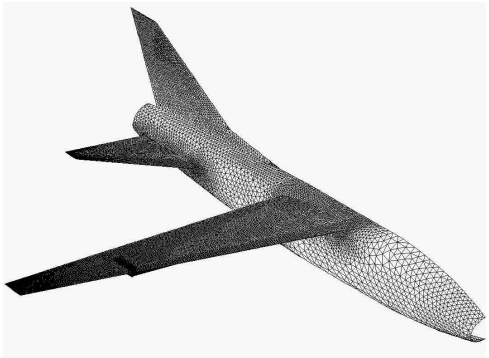

Figure 3: Surface triangulation of the simplified A7 SBW demonstrator aircraft geometry.

Figures 4 to 6 show the FELISA inviscid results of this flow solution. Figure 4 shows the pressure contour plots on the entire geometry. Figure 5 shows the pressure contours on the surface of the wing, while Figure 6 shows the pressure contours on the surfaces of the strut and pylon. From these plots, several observations can be made.

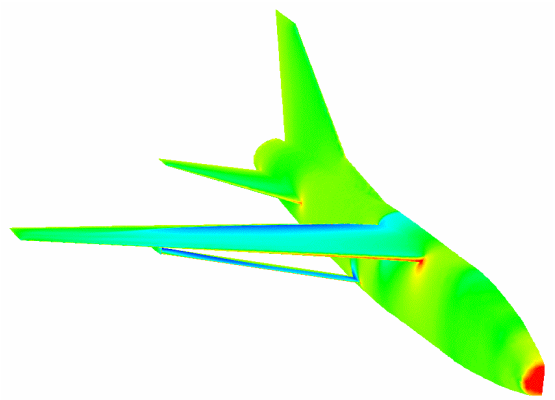

Figure 4: Pressure contours on the simplified A7 SBW geometry. FELISA inviscid solution, M=0.85, α = 2.85º.

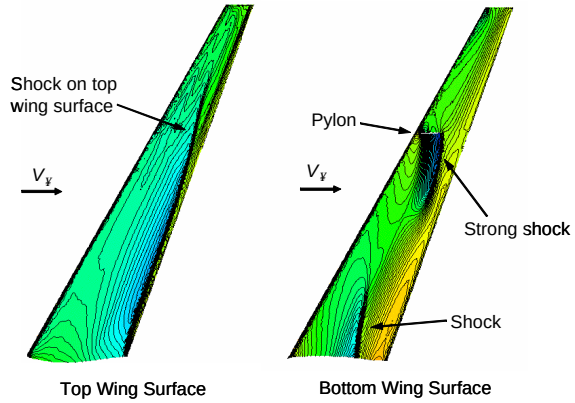

Figure 5: Pressure contours on the top and bottom surface of the wing on the simplified A7 SBW demonstrator aircraft. FELISA inviscid solution, M=0.85, α = 2.85º.

- There is a strong shock on the upper surface of the wing positioned close to the trailing edge of the wing. However, it must be noted that only the designed airfoils for the outboard sections were used in this geometry. For the inboard airfoils, a NASA SC(2)-0614 airfoil was used in the root section and a NASA SC(2)-0712 airfoil was used at the 15% span station. It can be expected that using the designed airfoils at the inboard sections would improve the pressure distribution on the upper surface of the wing. Viscous effects would also alter the pressure distributions.

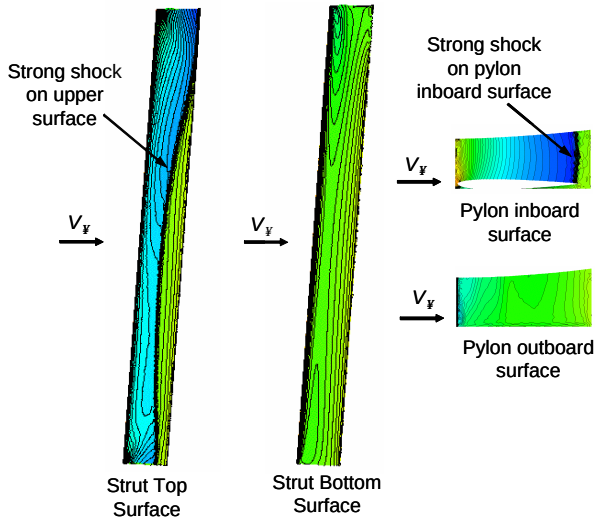

Figure 6: Pressure contours of the upper and lower surface of the strut and of the pylon inboard and outboard surface on the simplified A7 SBW demonstrator aircraft. FELISA inviscid solution, M=0.85, α=2.85º. Size of the pylon and strut shown here is not on the same scale

- There is a strong shock on the bottom surface of the wing close to the pylon, where the wing and the strut creates a 'channel effect' in the flow. This shock is positioned close to the trailing edge of the pylon.
- There is also a shock near the root on the bottom surface of the wing. This could be due to the wing/fuselage intersection. In a detailed design, this intersection with the fuselage would be designed to prevent this shock from appearing.
- The shock on the upper surface of the strut is strong and needs to be weakened considerably.
- The isobars on the upper surface of the strut are curved, and hence need to be designed to a more 'constant' distribution. The lower surface of the strut has a relatively more 'constant' distribution.

These observations identified areas where design changes needed to be made. The first change to the wing was to use specifically designed airfoils at the inboard and outboard control stations. Next, the airfoil sections for the pylon and strut were changed from NACA 0008 sections to an uncambered NASA supercritical airfoil. The SC(2)-0010 airfoil, with its trailing edge closed, and thickness scaled to a *t/c* of 8% was used. To close the airfoil's trailing edge, a 'sliver' of thickness was removed from the upper and lower surface to prevent introducing camber into the airfoil section.

We also know that the pylon toe, strut twist and incidence are key design considerations. The key question in the design process is determining the magnitude of these changes. With only one flow solution of the full configuration, there was no easy way of determining sensitivities to make changes.

4.2. Wing/strut/pylon only configuration studies

As mentioned earlier, to concentrate on the flow at the wing/strut/pylon juncture, and to reduce the design cycle time, we decided to consider wing/pylon/strut without the fuselage. Parametric studies were performed by changing the strut toe, strut incidence and strut twist. The results of these studies are not presented in this paper. A detailed discussion of this study can be found in reference [15]. The key conclusion from these parametric studies was that changing the pylon toe, strut twist and incidence resulted in only minor changes to the strong shock near the wing/pylon/strut intersection. It was clear that something other than the cumulative aerodynamic effect of the individual components was influencing the flow at this section.

4.3. The 'nozzle' effect

As we observed the pressure distributions results from the parametric studies, it became clear that the flow in the juncture was behaving like a nozzle. The flow was choking at a minimum area point at the intersection and expanding downstream, terminating in a strong shock near the trailing edge of the strut. To test this hypothesis, the area distribution which the flow 'sees' going through the intersection was computed. Since the area through the intersection is 'open' on one side (i.e. there is no wall bounding the intersection going towards the root), a fictitious spanwise wall was placed inboard of the pylon to bound the frontal area that the flow 'sees'. Note that this fictitious wall is only used for the purpose of calculating the frontal area, and does not affect the flow behavior. Figure 7 provides a graphical illustration of this area. The frontal three-dimensional area seemed more appropriate than the two-dimensional area across a spanwise cut near the intersection. This is because the airfoil shape of the pylon contributes to the area distribution. We subsequently examined the contribution of the pylon in more detail.

In our first analysis of the area effects on the flow properties through the juncture region, two different designs with different area distributions were made by changing the strut twist, the length of the pylon and the location of the pylon and strut relative to the wing. A reference design with a –3º strut twist was used as a comparator. Figure 8: Illustration showing the wing/pylon/strut intersection and how the frontal area distribution is calculated illustrates the geometric differences between the designs. Figure 9 gives the three-dimensional area distribution of the three different designs. Clearly, the second design has a smaller area distribution, and a shallower slope than the reference design. Also, the position of the minimum area is further aft in the second design compared to the reference. The third design has an increased area distribution, although the slope of the area distribution is similar to that of the reference design for most of the section. The position of the minimum area for the third design is closer to the leading edge of the strut than the other two designs.

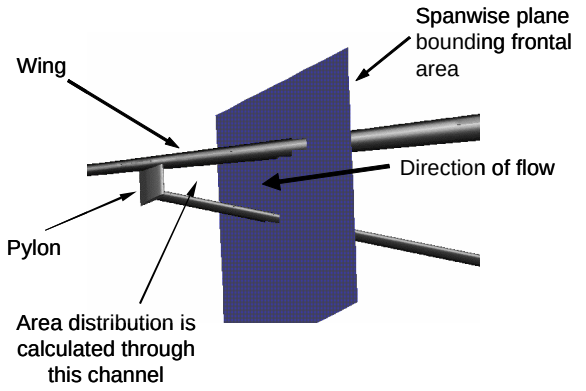

Figure 7: Illustration showing the wing/pylon/strut intersection and how the frontal area distribution is calculated

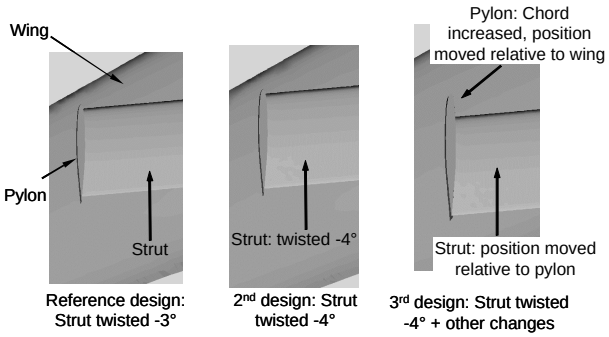

Figure 8: Illustration showing the wing/pylon/strut intersection and how the frontal area distribution is calculated

Figures 10 to 12 show the pressure coefficient distributions at the various stations on the strut obtained using FELISA. In Figure 10, we see that the strength of the shock was not reduced in any of the designs. The only net effect of the different designs was to move the position of the shock relative to the strut. As expected, the bottom surface of the strut does not seem to be affected by the change in the intersection area. We only observe the effects of twist on the bottom surface. Moving away from the junction, Figure 11 does not show the presence of any shock, as seen in the strut twist study. It is interesting that although the twist for

the second and third designs is the same, the effects of twist are amplified in the third design due to the change in pylon chord and, strut and pylon position. This same effect can be seen in Figure 12.

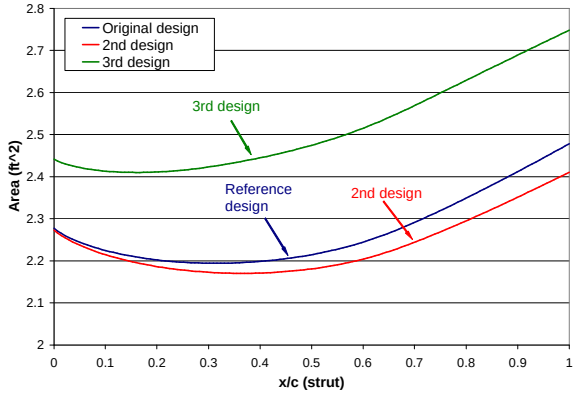

Figure 9: Three dimensional frontal area distribution through the wing/pylon/strut intersection of the different designs

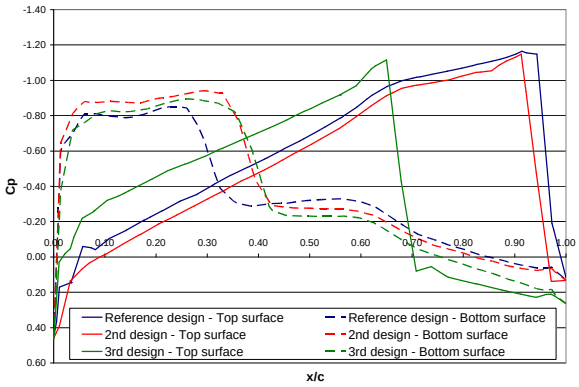

Figure 10: Pressure coefficient distribution on the strut at a spanwise cut close to the pylon. FELISA inviscid solution, M = 0.85.

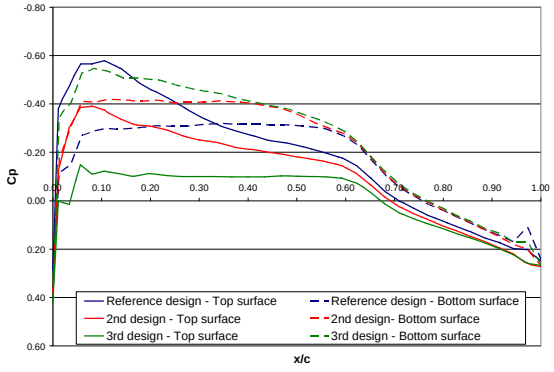

Figure 11: Pressure coefficient distribution on the strut at a spanwise cut mid-way between the pylon and the fuselage. FELISA inviscid solution, M = 0.85.

To test the hypothesis that the flow is choked at the minimum area location, the frontal area variation and the spanwise Mach number distribution near the pylon were examined. Noted that the area distribution represents the two dimensional frontal area that the flow 'sees' (as illustrated in Figure 9), while the Mach number distribution is that along a spanwise cut on the strut near the pylon. Figure 13 shows the result of this comparison. The flow reaches a Mach number of 1 close to or at the location of minimum area, confirming our hypothesis that the flow is behaving as if it were the flow through a nozzle. This also explains why changes in the pylon toe, strut twist and incidence barely affected the strength of the shock.

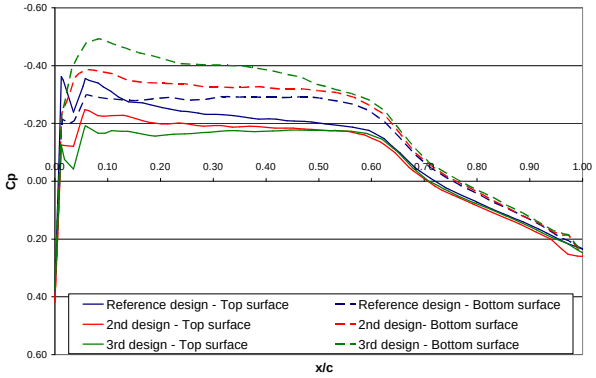

Figure 12: Pressure coefficient distribution on the strut at a spanwise cut near the fuselage. FELISA inviscid solution, M = 0.85.

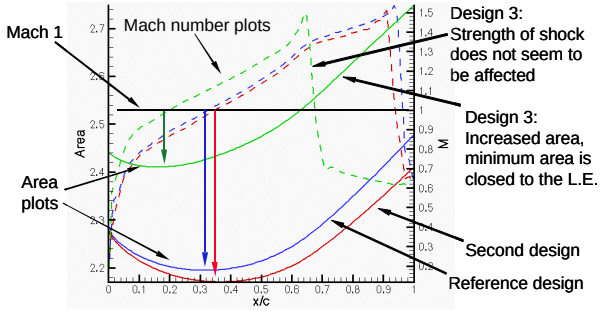

Figure 13: Frontal intersection area and surface flow Mach number cross plot. Colored arrows indicate the sonic location in relation to the area distribution

4.4. Effect of the pylon

Next, we considered the impact of the pylon on the intersection flow. We postulated that if the pylon had a large impact on the strength of the shock through the intersection, perhaps the use of a slotted pylon would relieve the accelerating flow through the intersection and reduce the strength of the shock. As an 'extreme slot', we removed the pylon entirely from the model and did a flow analysis of the wing and strut alone, leaving a gap in the geometry where the pylon had

been. By comparing this flowfield with a configuration with a pylon, we could explicitly identify the effect of the pylon on the flow through the intersection.

Figure 14 shows the results of this comparison for a pressure distribution at a spanwise cut on the strut near the original pylon location. We see that there is only a small reduction of the strength of the shock due to the absence of the pylon. The position of the shock does move forward by about 10% of the chord. Thus the pylon has a minor effect on the flow. Because the pylon has a minor effect, and the strut sweep is small (4.1°), the nozzle-like flow through the intersection is even more two-dimensional-like than first thought. This is a favorable finding since now we only need to change the two-dimensional area distribution between the strut and wing to affect the flow characteristics.

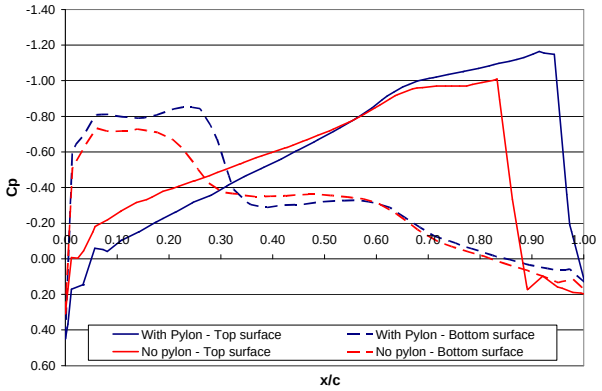

Figure 14: Pressure coefficient distribution on the strut close to the pylon (or lack thereof). This plot shows the effect the pylon has on the flow at the wing/pylon/strut intersection. FELISA inviscid solution, M = 0.85.

4.5. Solving the 'nozzle' effect

Having established a conceptual model for the cause of the flow acceleration through the wing/pylon/strut intersection, geometric changes can be made to weaken the shock at this location. One way to do this is to prevent the flow from choking by increasing the area at the throat, or in this instance, the location of minimum area, to an extent that the ratio of A/A*, which is the ratio of the inlet area to the throat area, is less than the critical 'choking' value of 1.027 (calculated at M=0.85). Figure 15 shows the orientation of the strut and wing sections at a spanwise cut near the pylon. Most of the change in area occurs due to the upper surface of the strut. Hence, if the strut upper surface were made flat, there would be little variation in the area distribution as the flow passes between the strut and the wing.

Two designs were made where the upper surface of the strut near the pylon was flattened. In the first design, the strut tip airfoil section thickness was halved,

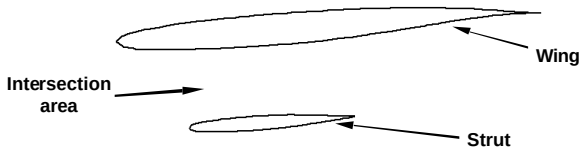

Figure 15: Illustration shows a spanwise cross section of the wing and strut near the pylon.

keeping the lower section geometry while leaving the upper portion flat. This essentially reduces the airfoil thickness by half from 8% to 4% *t/c*. At the strut root, the symmetric airfoil section remained unchanged, and the strut airfoil sections were obtained by a straight-line wrap between tip and the root sections. Note that the airfoil section at the strut tip has a sharp leading, due to the intersection between the lower half of the airfoil and the flat top. Therefore, we expect to have a pressure peak at the leading due to this sharp leading edge. The second design builds on the first design. At the strut tip for this design, the upper surface of the airfoil section is kept flat, and thickness is added to the lower surface to increase the strut thickness back to 8% *t/c*. The leading edge of this airfoil section was also rounded. A comparator case was also analyzed; keeping to the same design except using the symmetric airfoil section at the strut tip. Figure 16 shows the cross section differences between all three designs.

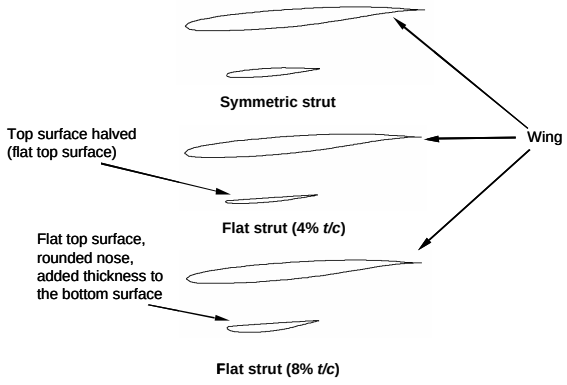

Figure 16: Illustration shows a spanwise cross section near the pylon of three different designs that were created to reduce and eliminate the strong shock at the wing/pylon/strut intersection.

Figure 17 shows the strut upper surface contour comparisons between the 3 different designs. The shock strength was weakened considerably in the 4% *t/c* flat strut design, and eliminated it in the 8% *t/c* flat strut design. Figure 18 gives the strut pressure coefficient distributions along a spanwise cut close to the pylon. As seen from the pressure contours, the strong shock on the upper surface of the strut was considerably weakened for the 4% *t/c* flat strut design and eliminated for the

8% *t/c* flat strut design. Also, as expected, there is a sharp pressure spike at the leading edge of the 4% *t/c* flat strut design. In the 8% *t/c* flat strut design this spike is reduced in magnitude due to the rounding of the leading edge of the tip strut airfoil. Several observations should also be made about the bottom surface pressure coefficient distribution of the strut. A strong shock appears on the bottom surface of the 8% *t/c* flat strut design. This is due to the extra thickness that was added to restore the required strut thickness. Airfoil shaping on this bottom surface should result in the weakening of the shock to an acceptable level. Also, for both the 4% *t/c* and 8% *t/c* flat strut designs, the strut is producing negative lift. Based on the strut incidence and strut twist studies, we feel that by adjusting the incidence and twist of the strut, it can be unloaded (a required design condition).

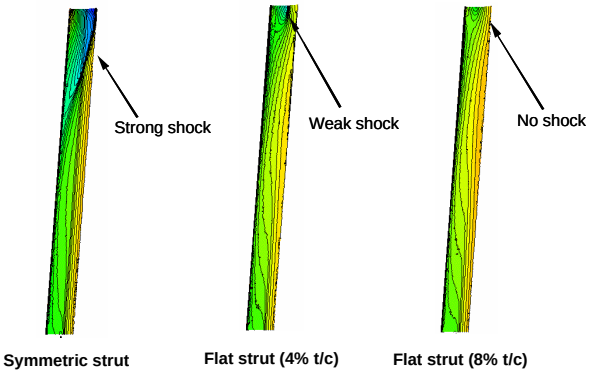

Figure 17: Pressure contours on the upper surface of the strut, comparing the reduction and elimination of the shock at the wing/pylon/strut intersection.

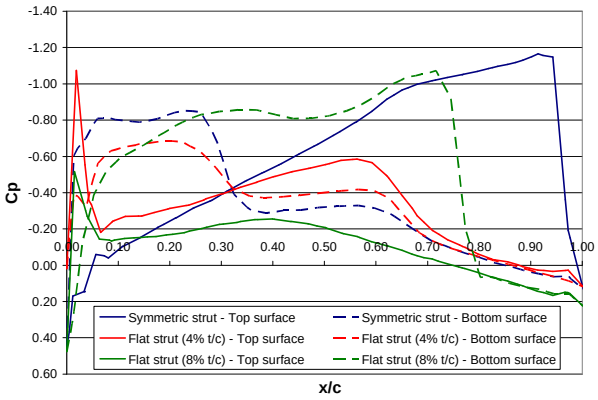

Figure 18: Pressure coefficient distribution on the strut at a spanwise cut near to the pylon. Plot compares the effect of the flattened strut top surface at near the wing/pylon/strut intersection. FELISA inviscid solution, M = 0.85.

Figure 19 shows the pressure coefficient distribution on the pylon for the three designs that were analyzed. As seen on the strut, the shock on the inboard surface of the pylon is weak for the 4% *t/c* flat strut design and is eliminated for the 8% *t/c* flat strut design. Note also that on the outboard surface of the pylon, the 8% *t/c* flat strut design produced a weak shock at about the 0.75 *x/c* location. As with the strut, we believe that changing the pylon toe can unload the pylon.

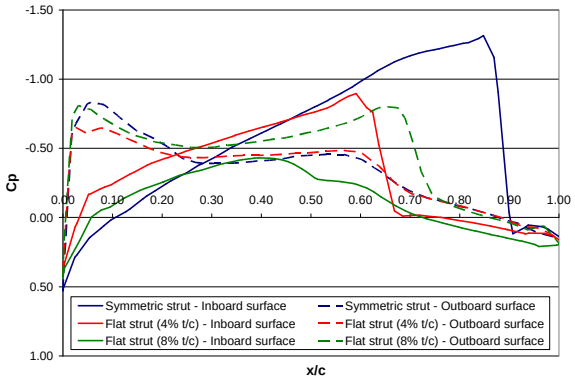

Figure 19: Pressure coefficient distribution on the pylon. Plot compares the effect of the flattened strut top surface near the wing/pylon/strut intersection. FELISA inviscid solution. M = 0.85.

5. Conclusions

We used an Euler analysis to investigate the transonic aerodynamic interference flowfield of a wing/pylon/strut juncture. In general, a strong shock may arise between the top of the strut and the bottom of the wing. The key finding was that the strong shock formed at the wing/pylon/strut intersection because the flow at the juncture behaves like that through a two-dimensional nozzle. With this understanding, we showed that the shock strength can be reduced or even eliminated by flattening the upper surface of the strut near the intersection to reduce the effective area ratio below the critical value. The presence of the pylon did not contribute to the key features of the interference. Although viscous effects were not taken into account in this study, previous studies have shown that the viscous effects reduces the strength of the shocks that form at this intersection.

6. Acknowledgements

The Systems Analysis Branch at NASA Langley supported our work. We would also like to acknowledge several people for their direct and indirect contribution to this project: Dick Campbell and Francis Capone at NASA Langley for their valuable insight, Andrew Hahn from NASA Ames for his help with the grid generation, Karen L. Bibb at NASA Langley for

her help on using the FELISA system, and, Andrew Parker and Dan McCormick at Virginia Tech for their help with this work. Prof. Mark Drela of MIT provided MSES to us.

7. References

[1] Pfenninger, W., "Design Considerations of Large Subsonic Long Range Transport Airplanes with Low Drag Boundary Layer Suction," Northrop Aircraft, Inc., Report NAI-58-529 (BLC-111), 1958. (Available from DTIC as AD 821 759)

[2] Grasmeyer, J.M., Naghshineh_Pour, A., Tetrault, P.-A., Grossman, B., Haftka, R.T., Kapania, R.K., Mason, W.H., Schetz, J.A., "Multidisciplinary Design Optimization of a Strut-Braced Wing Aircraft with Tip-Mounted Engines," MAD 98-01-01, 1998.

[3] Grasmeyer, J.M., "Multidisciplinary Design Optimization of a Strut-Braced Wing Aircraft," MS Thesis, Virginia Polytechnic Institute & State University, April 1998.

[4] Grasmeyer, J.M., "Multidisciplinary Design Optimization of a Transonic Strut-Braced Wing Aircraft," *37th AIAA Aerospace Sciences Meeting and Exhibit*, Reno, NV, Jan 11-14, 1999, AIAA Paper 99-0010.

[5] Gundlach, J.F., Tetrault, P.A., Gern, F., Nagshineh-Pour, A., Ko, A., Schetz, J.A., Mason, W.H., Kapania, and R.K., Grossman, B, "Multidisciplinary Design Optimization of a Strut-Braced Wing Transonic Transport," AIAA 2000-0420, 2000.

[6] Ko, A., "The Role of Constraints and Vehicle Concepts in Transport Design: A Comparison of Cantilever and Strut-Braced Wing Airplane Concepts," MS Thesis, Virginia Polytechnic Institute & State University, April 2000.

[7] Gern, F.H., Sulaeman, E., Naghshineh-Pour, A., Kapania, R.K., and Haftka, R.T., "Flexible Wing Model for Structural Wing Sizing and Multidisciplinary Design Optimization of a Strut-Braced Wing,", *41st AIAA/ASME/ASCE/AHS/ASC Structures, Structural Dynamics, and Materials Conference and Exhibit*, Atlanta, GA, April 3-6,2000. AIAA Paper 2000-1427

[8] Tetrault, P.-A., Schetz, J. A., and Grossman, B., "Numerical Prediction of the Interference Drag of a Streamlined Strut Intersecting a Surface in Transonic Flow," *38th Aerospace Sciences Meeting and Exhibit*, Reno, NV, Jan 10-13, 2000, AIAA Paper 2000-0509.

[9] Bartelheimer, W., Horstman, K. H., and Puffert-Meissner, W., "2-D Airfoil Tests Including Side Wall Boundary Layer Measurements", in *A Selection of Experimental Test Cases for the Validation of CFD Codes*, AGARD Advisory Report No. 303, 1994.

[10] Potsdam, M. A., Intemann, G. A., Frink, N. T., Campbell, R. L., Smith, L. A., and Pirzadeh, S., "Wing/Plyon Fillet Design Using Unstructured Mesh Euler Solvers", *AIAA Paper 93-3500*, 1993.

[11] Agrawal, S., Creasman, S. F., and Lowrie, R. B., "Evaluation of Euler Solvers for Transonic Wing-Fuselage Geometries", *Journal of Aircraft*, Vol. 28, No. 12, 1991, pp. 885-891.

[12] Tetrault, P.-A., "Numerical Prediction of the Interference Drag of a Streamlined Strut Intersecting a Surface in Transonic Flow," Ph.D. Dissertation, Virginia Polytechnic Institute & State University, January 2000.

[13] Ko, A., Mason, W. H., Grossman, B., Schetz, J.A., "A-7 Strut Braced Wing Concept Transonic Wing Design", VPI-AOE-275, Virginia Polytechnic Institute and State University, July, 2002.

[14] Lamar, J.E., "A Vortex Lattice Method for the Mean Camber Shapes of Trimmed Non-Coplanar Planforms with Minimum Vortex Drag," NASA TN D-8090, June 1976.

[15] Harris, C.D., "NASA Supercritical Airfoils: A Matrix of Family Related Airfoils", NASA TP 2969, March 1990.

[16] Peiro, J., Peraire, J., Morgan, K., *FELISA System Version 1.1 (Rev. 1) Reference Manual: Part 1-Basic Theory*, NASA Langley Research Center, VA, Nov., 1996.

[17] Drela, M. and Giles, M. B., "ISES: A Two-Dimensional Viscous Aerodynamic Design and Analysis Code," AIAA Paper 87-0424, 1987.

[18] Giles, M. B., and Drela, M., "Two-Dimensional Transonic Aerodynamic Design Method," *AIAA Journal*, Vol. 25, No. 9, 1987, pp. 1199-1206.

[19] Drela, M., and Giles, M. B., "Viscous-Inviscid Analysis of Transonic and Low Reynolds Number Airfoils," *AIAA Journal*, Vol. 25, No. 10, 1987, pp. 1347-1355.